

Numerical Prediction of DNB under Vertical and Inclined Condition with R134a Refrigerant

Giwon Bae, Hyoung kyu Cho*

Department of nuclear engineering, Seoul National Univ., 1 Gwanak-ro, Gwanak-gu, Seoul 08826

*Corresponding author: chohk@snu.ac.kr

*Keywords: DNB, Multiphase CFD, Inclined condition, R134a refrigerant, condensation model, Star-CCM+

1. Introduction

Recently, as the reduction of greenhouse gases has become a significant concern in the marine industry, interest in FNPPs (floating nuclear power plants) has been increasing [1]. FNPPs have advantages such as the capability to supply electricity to remote areas and low carbon emissions. However, compared to land-based nuclear reactors, FNPPs experience inclinations and motion conditions that influence the thermal-hydraulic behavior of the reactor. Within the existing scholarly literature, an insufficiency is observed in experiments or models elucidating variations in CHF in response to changes in ocean conditions. Motivated by this, experiments were conducted by SNU using the R134a refrigerant as a simulant fluid to investigate CHF behavior under ocean conditions [2].

Meanwhile, various multiphase CFD methodologies have been developed to predict CHF with water. Among them, the CASL program [3] has devised an advanced methodology considering interphase momentum transport and bubble size distribution using Star-CCM+ software [4]. However, since this methodology has yet to be validated under inclined and motion conditions, it needs validation to predict the FNPPs' CHF.

This study introduced a modified CFD methodology to predict CHF under inclination using R134a. As an initial step of comprehending the changes in multiphase flow phenomena under ocean conditions, calculations were validated under vertical and inclined conditions. Among the available databases, the cases with 2.515 MPa of pressure and DNB-type conditions were selected for validation

2. Numerical Methods

This section provides the boiling model used in this calculation and describes the differences with CASL FY19 models. The geometry configuration of the test section of the SNU experiment, experimental conditions, and calculation methodology are also detailed.

2.1 Star-CCM+ Eulerian multiphase approach

In this study, the Star-CCM+ software was used. Star-CCM+ provides the Eulerian multiphase (EMP) approach to simulate multiphase flow. This framework assumes that two fluids (liquid and vapor) coexist inside each cell. Mass, momentum, and energy equations are

solved for each phase. The governing equation is expressed in Eq. (1), (2), and (3) in Table I.

Table I: Governing Equation of EMP approach

Mass conservation	
$\frac{\partial(\alpha_k \rho_k)}{\partial t} + \nabla \cdot (\alpha_k \rho_k \mathbf{u}_k) = \Gamma_k$	(1)
Momentum conservation	
$\frac{\partial(\alpha_k \rho_k \mathbf{u}_k)}{\partial t} + \nabla \cdot (\alpha_k \rho_k \mathbf{u}_k \mathbf{u}_k) = -\nabla(\alpha_k \rho_k) + \nabla \cdot (\alpha_k \boldsymbol{\tau}_k) + \alpha_k \rho_k \mathbf{g} + \mathbf{M}_k^i$	(2)
Energy conservation	
$\frac{\partial(\alpha_k \rho_k e_k)}{\partial t} + \nabla \cdot (\alpha_k \rho_k \mathbf{u}_k e_k) = -\nabla(\alpha_k \rho_k) + \nabla \cdot (\alpha_k \boldsymbol{\tau}_k) + \alpha_k \rho_k \mathbf{g} + E_k^i$	(3)

Γ_k represents an interfacial mass transfer of each phase, and \mathbf{M}_k^i represents an interfacial momentum transfer. In Star-CCM+, energy transfer is calculated with Γ_k and latent heat, so E_k^i is the same as $h_{lv} \Gamma_k$. These terms can be calculated with various models and field functions.

A modified heat partitioning model [5] was adopted to simulate wall boiling phenomena. The heat partitioning model is expressed in Eq. (4) ~ (8) in Table II.

Table II: Wall heat partitioning model in this study

Total heat flux	
$\begin{cases} q''_{tot} = q''_c + q''_q + q''_e \\ q''_{DNB} = q''_v \end{cases}$	(4)
Liquid convection	
$q''_c = \frac{\rho_l c_{pl} u_l^*}{t_l^*} (T_w - T_l)$	(5)
Quenching heat flux	
$q''_q = 2K_q f \sqrt{\frac{\rho_l c_{pl} k_l t_w}{\pi}} (T_w - T_l)$	(6)
Evaporation heat flux	
$q''_e = N'' f \frac{\pi D_b^3}{6} \rho_g h_{lv}$	(7)
Vapor convection	
$q''_v = \frac{\rho_v c_{pv} u_v^*}{t_v^*} (T_w - T_v)$	(8)

As shown in Table II, a modified wall dryout model was used to simulate rapid temperature increase. This heat partitioning model assumes a situation in which all heat is transferred to vapor convection.

2.2 Comparison between CASL and this study

This study used a modified mass and momentum transport model with CASL. A comparison between CASL and this study is provided in Table III. The

differences between CASL and this study are highlighted in bold.

Table III: Comparison between CASL and this study

	Parameters	CASL FY 19	This study
Turbulence Model	Turbulence	Standard k-epsilon linear	Standard k-epsilon linear
Interaction length scale	Interaction length scale	Modified S-gamma (Partially mobile interface)	Modified S-gamma (Fully mobile interface)
	Interaction area density	Symmetric	Symmetric
Interfacial momentum transfer	Drag coefficient	Tomiyama (Moderate contaminate)	Tomiyama (Clean)
	Drag correction	Volume fraction exponent (0.0)	Simmonet correction
	Lift coefficient	Sugrue	Sugrue
	Wall lubrication force	Lubchenko	Lubchenko
Wall boiling	Departure diameter	Kocamusta-faogullari	Kocamusta-faogullari
	Departure frequency	Cole	Cole
	Nucleation site density	Li et al.	Li et al.
	Bubble influence area	Del Valle kenning (0.8)	Del Valle kenning (0.8)
	DNB detection	Analytical wall dryout	$\alpha_v > 0.8$ $y^+ : 0 \sim 200$
Interfacial heat transfer	Condensation fluid	Kim-Park	Issa et al.
	Condensation Vapor	$Nu_v = 26$	$Nu_v = 26$

The drag coefficient was slightly different from the CASL FY19 framework. First, the option for the drag coefficient was changed. Tomiyama [6] proposed three drag coefficients related to the liquid's purity and the bubble's shape. Since the SNU test used pure R134a refrigerant as a working fluid, a pure option was selected in this study. In addition to this, the drag correction model was changed. The CASL framework adopted a volume fraction exponent of 0.0. This correction results in the exact drag force calculation at high and low void fractions. This study used the Simmonet drag correction to calculate the drag force accurately in the high void fraction region.

Regarding bubble coalescence, Star-CCM+ provides four viscous coalescence rate models proposed by Lo and Zhang [7]. The fully mobile interface option was selected for the viscous coalescence model because it is appropriate for pure working fluid.

For interfacial heat transfer, Issa's condensation Nusselt number was used. Eq. (9) and (10) provide the

two condensation Nusselt numbers used in CASL and this study.

$$Nu_c = 0.2575 Re_b^{0.7} Ja_1^{-0.2043} Pr_1^{-0.4564} \quad [8] \quad (9)$$

$$Nu_c = 4.34 Re_b^{0.89} Pr_1^{0.333} \quad [9] \quad (10)$$

The Kim-park correlation Eq. (9) contains Jakob number in the Nusselt number. However, R134a has a latent heat equivalent of about 0.1 times that of the water. Therefore, a correlation with Jakob number is inappropriate for simulation using refrigerant as a working fluid. Thus, Issa's correlation Eq. (10) was selected in this study.

2.3 Experimental condition & calculation methodology

For the validation calculation, the CHF experiments conducted under inclination, named NEOUL-R, were simulated. It has a single annulus test section with an electrical heater at the center. Figure 1 shows the geometry and mesh distribution of the test section.

Three different mesh sizes are utilized: coarse mesh (58,800), standard mesh (117,600), and fine mesh (235,200). The standard mesh (117,600) was chosen after checking the void fraction and temperature of the heated section. The Y^+ of all meshes is between 50 and 200. ($[N_r, N_\theta, N_z] = [7, 80, 210]$)

High mass flux conditions were selected since the EMP model is appropriate for DNB calculation. The experimental condition used in the simulation is shown in Table IV.

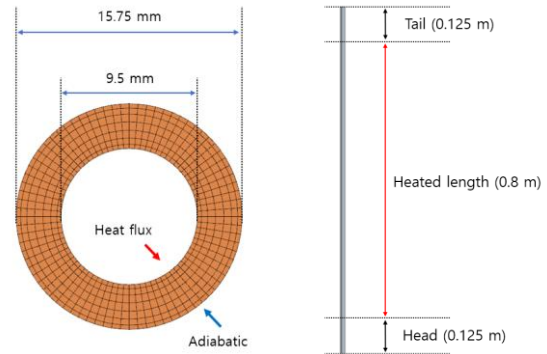


Figure 1. Geometry & Mesh distribution of test section

Table IV: Experimental condition

Parameter	Range
Pressure	2.515 MPa
Inlet subcooling	23 ~ 37 K
Mass flux	900 ~ 1800 kg/m ² s
Inclination	Vertical: 0°, Inclined: 30°, 45°

The reference pressure was set at 2.515 MPa to simulate pressure. In addition, the liquid and vapor phase properties were implemented with a table. Inlet

subcooling and mass flux can be easily implemented with boundary conditions.

The inclination angle of the test section is simulated with gravity term. If the test section is tilted by θ radians, the gravity vector is calculated with Eq. (11).

$$\mathbf{g} = [0, 9.81 \sin \theta, -9.81 \cos \theta] \quad (11)$$

For the CHF calculation, a stepwise heat flux was applied for the stability of the calculation. Uniform heat distribution was used in this calculation. Figure 2 shows the heat flux, maximum wall superheat, and void fraction.

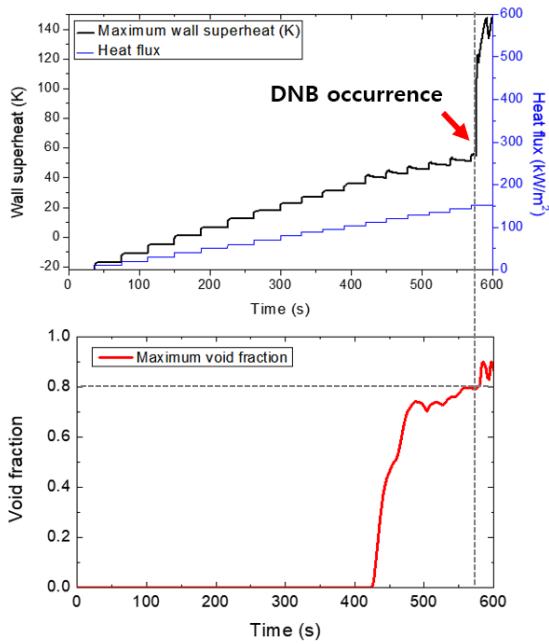


Figure 2. CHF calculation method

As shown in Figure 2, the heat flux was increased every 30 seconds. With wall superheat and void fraction, CHF can be detected. The void fraction is used to distinguish whether the temperature divergence is caused numerically rather than by CHF. The occurrence of CHF was evaluated when the void fraction exceeded 0.8 and there was a temperature excursion.

3. Calculation Results

3.1 CHF under the vertical and inclined conditions

A quantitative comparison between calculated CHF values and the corresponding experimental results is conducted. The results shown in Figures 3 and 4 illustrate that the calculated CHF from CFD matches well with the experiment for both vertical and inclined conditions. The maximum deviation for each inclination angle was about 20%.

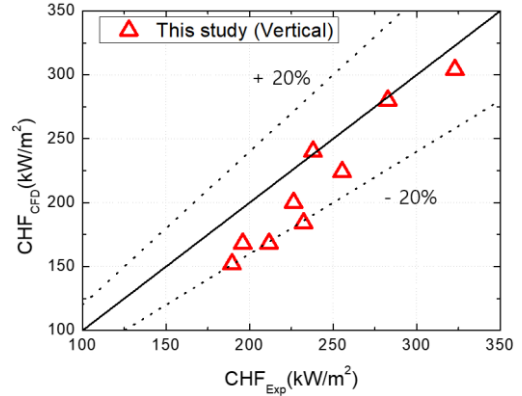


Figure 3. Calculated CHF compared with measured CHF at the vertical test section

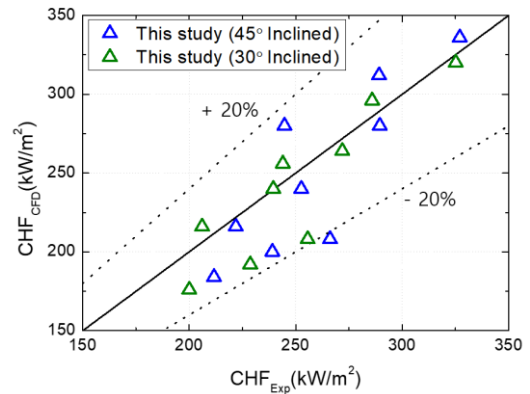


Figure 4. Calculated CHF compared with measured CHF at the inclined test section

3.2 CHF enhancement effect under the inclined condition

Based on the NEOUL-R experimental database at 2.5 MPa, there is a tendency toward an increase in CHF within the DNB region. Figure 5 illustrates the comparison of the CHF enhancement effect between the experiment and CFD results.

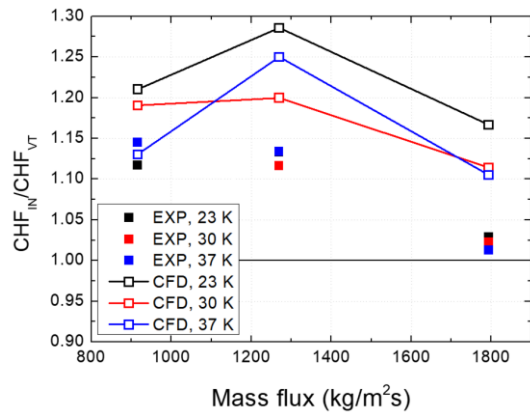


Figure 5. Comparison of CHF enhancement between experiment and CFD (45° inclined)

As shown in Figure 5, the experiment and CFD indicate an increase in CHF under inclined conditions

compared to vertical conditions. In the experiment, the CHF enhancement effect decreases as mass flux increases. This trend occurs because flow inertia has a greater influence than the vapor's buoyancy. However, the observed CHF enhancement trend in the CFD results slightly overestimated the experimental trend.

4. Discussion

With this framework, the void fraction can explain the physical mechanism for CHF enhancement. Under uniform heat flux, CHF occurs at the end of the heated length (EHL). Figure 6 shows the void fraction at EHL for both vertical and inclined conditions.

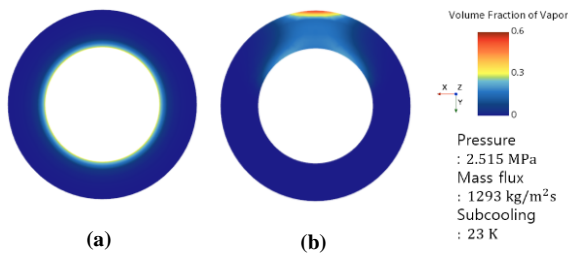


Figure 6. Void fraction at end of heated section at 160 kW/m^2 (a) Vertical (0°) (b) 45° Inclined

Figure 6 shows that the maximum void fraction at EHL for the inclined condition is higher than for the vertical condition. However, the void fraction near the wall region for the inclined condition is lower than for the vertical condition. Due to the combined force of the lift force and buoyancy, bubbles are separated from the heater and accumulate at the top of the tube. Since bubbles are removed from the heated section in an inclined condition, CHF increases.

The CASL framework underestimated the void fraction more than this study and overestimated the CHF of the NEOUL-R test section by more than 80% for both vertical and inclined conditions. Figure 7 compares the void fraction between this study and the CASL FY 19 model.

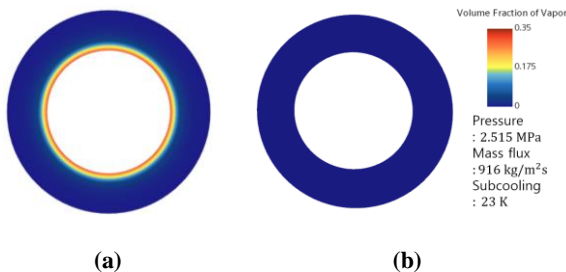


Figure 7. Void fraction at end of heated section at 160 kW/m^2 for vertical condition (a) This study (b) CASL

As shown in Figure 7, the void fraction near the wall region in this study is much higher than in the CASL model. This result can be explained by considering the differences in the condensation heat transfer model.

5. Conclusions

This study established multiphase CFD methodology for DNB, and validation calculations were performed for a NEOUL-R test section at 2.515 MPa. The calculation results matched well with experimental data for all inclination angles. However, the overestimation of CHF enhancement under inclined conditions in CFD was observed, and this trend magnified with increasing mass flux.

The CFD calculation results also explained the mechanism of CHF enhancement. The combined effect of lift force and buoyancy led to the separation of bubbles from the heater, causing a reduction in the void fraction near the heated section. Furthermore, it is confirmed that the CASL FY19 model overestimated the CHF of the NEOUL-R test section.

This study calculated the DNB for high-pressure (2.515MPa) refrigerants. However, this methodology has limitations in evaluating the liquid film dryout (LFD) region. Evaluation of dryout using CFD methodology is necessary for cases where the continuous phase is a gas. Additionally, an assessment of CHF over a wide pressure range is planned for future investigation.

ACKNOWLEDGMENT

This work was supported by the National Research Foundation of Korea (NRF) grant funded by the Korea government (MSIT) (No. RS-2022-00144494)

REFERENCES

- [1] IMO MEPC72, "Resolution MEPC.304(72)", Initial IMO Strategy on Reduction of GHG Emissions from Ships (2018).
- [2] G. W. Kim, Experimental investigation of critical heat flux on a single heater rod under inclined and rolling conditions, PhD thesis, Seoul National University, (2021).
- [3] J. Feng, R. Kommajosyula, E. Baglietto. "Finalize CASL Closure Models with Wall Model Improvements including Nucleation Site Density and Bubble Departure diameter." CASL Report CASL-U- 2019-2051-000. (2019).
- [4] "STAR-CCM+, version 2021.3", (2021).
- [5] N. Kurul and M. Z. Podowski, "On the Modeling of Multidimensional Effects in Boiling Channels," in Proc. of the 27th National Heat Transfer Conference, (1991).
- [6] A. Tomiyama et al. "Drag Coefficient of Single Bubble under Normal and Micro Gravity Conditions", JSME (1998).
- [7] Lo, S. and Zhang, D. "Modelling of Break-up and Coalescence in Bubbly Two-Phase Flows", J. Comp. Multiphase Flows (2009).
- [8] S.J. Kim, G.C. Park, "Interfacial heat transfer of condensing bubble in subcooled boiling flow at low pressure", International Journal of Heat and Mass Transfer, Volume 54 (2011).
- [9] S. Al Issa, P. Weisensee, R. Macián-Juan, "Experimental investigation of steam bubble condensation in vertical large diameter geometry under atmospheric pressure and different flow conditions", International Journal of Heat and Mass Transfer, Volume 70 (2014).
- [10] Brewster, R., "Application of Advanced DNB Methods at Westinghouse" CASL Report CASL-U-2018-1737-000. (2018)